A New Double-Moment Microphysics Parameterization for Application in Cloud and Climate Models. Part II: Single-Column Modeling of Arctic Clouds

H. MORRISON

Department of Aerospace Engineering, University of Colorado, Boulder, Colorado

J. A. CURRY

School of Earth and Atmospheric Science, Georgia Institute of Technology, Atlanta, Georgia

M. D. SHUPE AND P. ZUIDEMA

Cooperative Institute for Research in Environmental Sciences/NOAA ETL, Boulder, Colorado

ABSTRACT

The new double-moment microphysics scheme described in Part I of this paper is implemented into a single-column model to simulate clouds and radiation observed during the period 1 April–15 May 1998 of the Surface Heat Budget of the Arctic (SHEBA) and First International Satellite Cloud Climatology Project (ISCCP) Regional Experiment–Arctic Clouds Experiment (FIRE–ACE) field projects. Mean predicted cloud boundaries and total cloud fraction compare reasonably well with observations. Cloud phase partitioning, which is crucial in determining the surface radiative fluxes, is fairly similar to ground-based retrievals. However, the fraction of time that liquid is present in the column is somewhat underpredicted, leading to small biases in the downwelling shortwave and longwave radiative fluxes at the surface. Results using the new scheme are compared to parallel simulations using other microphysics parameterizations of varying complexity. The predicted liquid water path and cloud phase is significantly improved using the new scheme relative to a single-moment parameterization predicting only the mixing ratio of the water species. Results indicate that a realistic treatment of cloud ice number concentration (prognosing rather than diagnosing) is needed to simulate arctic clouds. Sensitivity tests are also performed by varying the aerosol size, solubility, and number concentration to explore potential cloud–aerosol–radiation interactions in arctic stratus.

1. Introduction

The importance of arctic clouds on the regional and global climate has been well documented (e.g., Curry 1995; Curry et al. 1996). Cloud parameterizations used in climate models have typically been developed for lower latitude regions. Thus, simulations of arctic cloudiness have generally fared poorly (e.g., Curry et al. 1996; Tao et al. 1996; Walsh et al. 2002). Problems in modeling these clouds have been hypothesized to arise from the complex vertical structure of the arctic boundary layer, the presence of leads (cracks) in the sea ice surface, the persistence of mixed-phase clouds, and the susceptibility to modification by aerosol (Curry et al. 1996). Difficulty in modeling and remotely sensing arctic clouds motivated the First International Satellite

Cloud Climatology Project (ISCCP) Regional Experiment–Arctic Clouds Experiment (FIRE–ACE), which used research aircraft to provide in situ cloud microphysical observations during April–July 1998 (Curry et al. 2000). FIRE–ACE was conducted in conjunction with the 1997–98 Surface Heat Budget of the Arctic Ocean (SHEBA) field project (Uttal et al. 2002).

Deficiencies have been indicated in simulations of cloudiness observed during SHEBA/FIRE–ACE. Single-column model (SCM) simulations of May 1998 show a substantial underprediction of the liquid water path (LWP; Curry et al. 2000). Morrison et al. (2003) conducted a detailed comparison of simulated column cloud properties with observations for the period 1 April to 16 May 1998. They found the model reasonably predicted the mean cloud boundaries and fraction, but had difficulty correctly partitioning the cloud phase, resulting in a substantial underprediction in mean LWP and the fraction of time liquid water was present. These biases were attributed to unrealistic modes of glaciation

Corresponding author address: Hugh Morrison, Dept. of Aerospace Engineering, University of Colorado, Boulder, CO 80309. E-mail: hugh@cloud.colorado.edu

in the model. Girard and Curry (2001) found that simulation of LWP in supercooled arctic stratus was improved with the addition of crystal and droplet number concentrations as prognostic variables.

Correctly predicting the LWP and cloud phase is crucial in climate simulations since liquid water dominates the arctic surface radiative fluxes (Shupe and Intrieri 2004; Zuidema et al. 2005), which in turn impact the sea ice mass balance (Curry and Ebert 1990). Observations suggest there is no simple temperature–phase relationship in supercooled arctic clouds. Lidar depolarization ratios indicated that liquid water was frequently present in clouds during SHEBA (Intrieri et al. 2002; Shupe and Intrieri 2004). Liquid water was observed during FIRE–ACE by in situ aircraft measurements at temperatures as low as $-23°C$, while ice was found at temperatures as warm as $-4°C$ (Curry et al. 2000). Curry et al. (1996) cite observations of arctic clouds that were completely glaciated at $-14°C$. Intrieri et al. (2002) infer the presence of liquid water at temperatures as low as $-34°C$ using lidar depolarization ratios measured during SHEBA.

Previous studies have indicated the importance of droplet and crystal sizes and number concentrations in determining the LWP and phase of cold clouds. Hobbs and Rangno (1998) and Rangno and Hobbs (2001) hypothesized that the occurrence of ice in slightly and moderately supercooled arctic clouds is related to the droplet size and number concentration. For example, clouds with a temperature in the range $-4°$ to $-10°C$ and a maximum droplet effective radius >12 μm (typically associated with a droplet number concentration less than 100 cm^{-3}) generally contained ice, while clouds with a smaller maximum effective radius (associated with a higher droplet number concentration) were typically ice free (Rangno and Hobbs 2001). Observations of polar maritime clouds suggested that glaciation was initiated by freezing of the largest drops (Hobbs and Rangno 1985; Rangno and Hobbs 1991). The formation of large drops may also lead to locally high water supersaturations and accelerated ice nucleation rates (Hobbs and Rangno 1990). The crystal concentration is important in supercooled clouds since it determines in part the phase relaxation time associated with ice. For example, when the ice concentration is high, phase relaxation is often short and the uptake of water vapor by the crystals occurs quickly. This enhanced Bergeron–Findeisen process (i.e., transfer of water vapor from droplets to crystals due to lower ice saturation compared to water saturation) can rapidly glaciate clouds (Hobbs and Rangno 1990). Crystal size also plays a role in the phase relaxation and is therefore an important parameter. Rauber and Tokay (1991) hypothesized that liquid water is maintained at the top of midlatitude, orographic mixed-phase clouds due to the presence of small crystals and thus slow phase relaxation.

Crystal and droplet concentrations and sizes are re-lated to the number of ice nuclei (IN) and cloud condensation nuclei (CCN) available. Since aerosol–cloud interactions in the Arctic are complex and have not been extensively studied, the physical processes controlling IN and CCN concentrations are not well understood (Curry 1995; Curry et al. 1996; Lohmann et al. 2001). The large sulfate component in arctic pollution aerosol (arctic haze) may deactivate ice-forming nuclei since sulfate particles act as poor IN (Borys 1989). However, solution drops containing an insoluble substrate may serve as IN after deliquescence (Ohtake 1993). CCN and IN may be depleted through nucleation and particle scavenging, which is particularly important in the stable arctic boundary layer with few in situ sources of aerosol at the ice-covered surface (Curry et al. 2000). Pinto (1998) hypothesized that liquid water was maintained in mixed-phase clouds observed during the Beaufort and Arctic Storms Experiment (BASE) due to the depletion of IN. Evidence of low IN concentrations in some mixed-phase stratus was suggested by small crystal concentrations ($\sim 1 L^{-1}$) observed during FIRE–ACE (Rogers et al. 2001). Several modeling studies have demonstrated the importance of IN concentration in determining the LWP and cloud phase (Harrington et al. 1999; Jiang et al. 2000; Girard and Curry 2001; Morrison et al. 2003). Lohmann et al. (2001) also found that the morphology and microphysical characteristics of arctic cirrus were highly sensitive to the number of IN and suggested that changes in the chemical and physical properties of aerosol can also influence ice clouds.

The new double-moment scheme described in Part I of this paper (Morrison et al. 2005, hereafter Part I) predicts the mixing ratios and number concentrations of droplets, cloud ice, snow, and rain and incorporates close coupling between the aerosol and cloud microphysics for both liquid and ice. Therefore, it is well suited for modeling arctic clouds that are frequently of mixed phase (Shupe and Intrieri 2004) and particularly susceptible to modification by aerosol (Curry 1995; Curry et al. 1996). In this study, the microphysics scheme is utilized in the Arctic Single Column Model (ARCSCM; Morrison et al. 2003) to simulate the 1 April to 15 May 1998 period of SHEBA/FIRE–ACE. We assume that the supersaturation and droplet activation are not resolved by the ARCSCM due to its coarse resolution and hence use the nonresolved version of the scheme (see Part I), which is appropriate for larger-scale models. We adopt the single-column modeling strategy described by Randall et al. (1996) and Randall and Cripe (1999). Single-column models, representing a single grid cell of a 3D climate model, allow for a first-order evaluation of physical parameterizations without added complications due to feedbacks with the large-scale dynamics. Since SCMs are computationally inexpensive, a parameterization may be tested over a wide range of conditions and parameter space. After the scheme is judged to have performed

reasonably in the SCM, it may then be implemented and tested in the 3D climate model.

The goal of this study is to determine the effectiveness of the ARCSCM in simulating arctic clouds and radiation using the new microphysics scheme. Model output is compared to detailed observations and ground-based retrievals obtained during SHEBA/FIRE–ACE. Results are also compared with parallel simulations using a number of other microphysics schemes of varying complexity to reveal improvements using the new scheme. Finally, sensitivity tests are described that assess how the model responds to changes in the specified aerosol properties. Since cloud phase and LWP are particularly important climatologically due to their impact on the surface radiative fluxes and energy balance, our analysis primarily focuses on these parameters.

2. Observations

SHEBA is described in detail by Uttal et al. (2002). A heavily instrumented icebreaker was frozen into the multiyear sea ice on 1 October 1997 at 75.27°N, 142.68°W and allowed to drift for one year across the Beaufort and Chukchi Seas. SHEBA was coordinated with the Atmospheric Radiation Measurement (ARM) program (Stokes and Schwartz 1994).

Temperature and relative humidity profiles at SHEBA were measured by rawinsondes launched two to four times per day. A Nipher shielded snow gauge system measured total precipitation accumulations on a daily basis (or as new precipitation warranted). The precipitation data were corrected by the SHEBA Project Office to account for various factors of the high-latitude environment (e.g., blowing snow). Surface and near-surface meteorological conditions were obtained from measurements taken on or near the Atmospheric Surface Flux Group tower (Persson et al. 2002).

Cloud properties were retrieved from a collection of ground-based instruments deployed at the SHEBA ice camp. A vertically pointing, 35-GHz, millimeter cloud radar (MMCR) made continuous measurements of reflectivity and mean Doppler velocity up to a height of 13 km. Collocated with the MMCR were a dual-channel microwave radiometer (MWR) used for simultaneous retrievals of LWP and precipitable water vapor (Westwater et al. 2001) and a depolarization lidar used to remotely determine cloud boundaries and phase (Intrieri et al. 2002). Retrieval techniques for estimating the liquid and ice water contents are described in Shupe et al. (2001). Relative uncertainty for the retrieved ice water content (IWC) is 60%–70% (Shupe et al. 2001). Instrument noise and retrieval uncertainty contribute to an instantaneous uncertainty of 25 g m^{-2} for the MWR-derived LWP (Westwater et al. 2001). Uncertainties associated with the time-averaged quantities described in this paper are expected to be somewhat

reduced due to the statistical nature of the retrievals (Morrison et al. 2003).

Radar retrievals of liquid water content (LWC) and droplet size were not performed for mixed-phase clouds (which occurred frequently during the period) since ice tends to dominate the radar signal. Estimates of LWC have been made by assuming adiabatic ascent of a parcel from the lidar-determined cloud base and constraining the column-integrated values to MWR retrievals (Zuidema et al. 2005). Droplet effective radius is determined from the constrained adiabatic LWC profiles and an assumed size distribution dispersion and number concentration based on aircraft measurements obtained on 4 and 7 May during FIRE–ACE (Zuidema et al. 2005). Uncertainty in the LWC profiles is estimated to be about 0.05 g m^{-3}. Comparisons with in situ aircraft data validate this multisensor/adiabatic approach for determining the liquid microphysical parameters (Zuidema et al. 2005).

Cloud boundaries are based on combined MMCR and lidar data (Intrieri et al. 2002). In general, the lidar was used to determine the cloud base since the radar also responds to precipitation. The cloud top was determined by radar since the lidar was often attenuated within the cloud. Various cloud fractions (separated by type and altitude) are based on radar measurements and cloud type classifications that include lidar data.

In situ cloud and aerosol microphysical properties were obtained from an array of instruments flown on the NCAR C-130Q aircraft as part of FIRE–ACE. These instruments are detailed in Curry et al. (2000), Lawson et al. (2001), Zuidema et al. (2005), and Yum and Hudson (2001). The droplet number concentration was determined from a Forward Scattering Spectrometer Probe (FSSP). Total aerosol concentration is determined from condensation nuclei (CN) measurements (Yum and Hudson 2001). Aerosol properties are inferred from observed CCN activity spectra (i.e., number of CCN as a function of the supersaturation; Yum and Hudson 2001) as described in section 4.

All of the water paths, contents, sizes, and number concentrations presented here are combinations of cloud water and precipitation. Hereafter, LWP will refer to the combined rain and cloud water paths, LWC to the combined cloud and rainwater contents, IWP to the combined cloud ice and snow water paths, and IWC to the combined cloud ice and snow water contents, for both modeled and retrieved values.

3. SCM description

Simulations of the atmospheric column during SHEBA were conducted using the new microphysics scheme (see Part I) implemented into ARCSCM. ARCSCM was developed by Morrison et al. (2003) for the purpose of evaluating physical parameterizations and studying 1D thermodynamic interactions that occur

over the multiyear sea ice of the Arctic Ocean. Prognostic variables include temperature, T, and water vapor mixing ratio, q_v, in addition to the quantities predicted by the microphysics scheme (mixing ratios and number concentrations of droplets, cloud ice, rain, and snow). Shortwave radiative transfer is treated using the two-stream delta–Eddington method of Briegleb (1992). Longwave radiative transfer is given by the Rapid Radiative Transfer Model (RRTM; Mlawer et al. 1997). The boundary layer and turbulence parameterization is a first-order nonlocal scheme described by Holtslag and Boville (1993). Sensible and latent heat fluxes over the ice-covered surface are calculated following Schramm et al. (1997).

As in other single-column models, horizontal advection and 3D winds must be specified in the ARCSCM. Vertical advection of scalar quantities (droplet and cloud ice mixing ratios and number concentrations) is calculated using a first-order forward scheme following the Arctic Regional Climate System Model (ARCSyM; Lynch et al. 1995). Vertical advection of precipitation (rain and snow) is neglected since the fall speeds associated with these particles are much greater than the specified vertical velocity. Horizontal advection of cloud water and precipitation is neglected due to lack of observations.

The cloud microphysics and radiation parameterizations are fully coupled using particle sizes diagnosed from the predicted number concentrations and mixing ratios. Liquid and ice hydrometeor optical properties are calculated following Slingo (1989) and Ebert and Curry (1992), respectively. Single-scattering albedo and asymmetry parameter are appropriately weighted by the optical depth associated with droplets and cloud ice predicted by the model. Precipitation (snow and rain) is neglected in solar radiative transfer but included in longwave calculations. Turbulent diffusion of scalars is calculated using an implicit solver (Grell et al. 1995). Turbulent mixing of precipitation (rain and snow) is neglected. Fractional cloudiness within the column is not considered; instantaneous cloud fraction is 1, if any model level has a condensed water content greater than 10^{-5} g m^{-3}, and 0 otherwise, following the ARCSyM. The parameterization of shallow and deep cumulus is not included since convection over arctic sea ice is limited with the exception of convective plumes emanating from leads (e.g., Pinto and Curry 1995). Since ARCSCM does not have a parameterization for subgrid-scale cloudiness, it is assumed that the model is able to resolve stratiform clouds using grid-scale values of relative humidity. Fractional and subgrid-scale cloudiness may be less important in the Arctic compared to lower latitudes since cloud systems in the region tend to be horizontally extensive (e.g., Curry and Herman 1985). However, vertical resolution is relatively important since arctic clouds often occur in horizontally extensive but vertically thin layers with sharp gradients in humidity above cloud top (Curry and Her-

man 1985; Morrison et al. 2003). These issues should be kept in mind when assessing the performance of the model.

4. Model configuration and forcing

The ARCSCM simulations described here are run with a vertical domain from the surface to 50 mb, with 27 levels and increasing vertical resolution toward the surface (~200 m in the lowest 1 km). The time step is 5 min. The ARCSCM is run in forecast mode using 72-h simulations. This approach helps to minimize model drift that might occur if the model was run with a single forecast over the entire 1 April to 15 May period of interest. Simulations are initialized using profiles of T and q_v constructed from rawinsonde and tower data. Owing to uncertainties in the vertical distribution of cloud water, the initial variables are set to zero, resulting in a finite spinup time for the model to produce clouds. The sonde relative humidity (RH) measured with the Vaisala RS80-H humicap sensor may be prone to a dry bias (e.g., Wang et al. 2002; Turner et al. 2003). These RH errors include both systematic and temperature-dependent (mostly at temperatures $<-30°$C) biases (Wang et al. 2002). Systematic dry biases are apparent in the SHEBA sondes since RH generally reached a maximum of only 90%–95% even when liquid water was indicated by retrievals. To account for these systematic biases, the tropospheric relative humidity profile measured by each sonde is adjusted so that it reaches a maximum of 100% if liquid water was indicated by the retrievals (the mean RH adjustment is 8.2%). When liquid water was not indicated, the mean adjustment value is applied to the sonde RH profile. To account for temperature-dependent errors, we use the temperature-dependent correction factor described by Wang et al. (2002) applied to levels where the temperature was below $-30°$C. Incorporating this temperature-dependent correction means that the sonde RH is adjusted more in the mid and upper troposphere than in the lower troposphere. Owing to uncertainties in the initial RH and the finite spinup time to produce cloud water, only hours 24–71 of the 72-h forecasts are archived, with the first 24 h omitted. Three-day forecasts are thus run for every two days so that hours 24–71 of the forecasts are concatenated to produce a continuous time series over the period 1 April to 15 May.

Hourly profiles of horizontal advection and wind and vertical velocity for the column overlying the SHEBA site were obtained from hours 12–35 of 36-h forecasts using the European Centre for Medium-Range Weather Forecasts (ECMWF) model version 13R4 with a nominal grid spacing of 60 km (Beesley et al. 2000). The ECMWF forcing is used since advection and vertical velocity could not be derived from SHEBA observations (sondes were launched from a single site only). The analysis of Morrison and Pinto (2004) showed substantial biases in the ECMWF advective

forcing for the SHEBA column, which is not surprising given the lack of observational data for over the Arctic Ocean. To account for these biases, the ECMWF advective tendencies are constrained to SHEBA observations following the method described by Morrison and Pinto (2004). Even though biases in the constrained advection still occur over periods of a few days, they are consistent with observations over periods of 1 month or more. Since a statistical evaluation of the ARCSCM over a 1.5-month period is given here, we assume that biases in the constrained ECMWF forcing do not play a significant role in the analysis. A detailed evaluation of the constrained forcing is given by Morrison and Pinto (2004).

Surface temperature, albedo, and pressure are specified from SHEBA observations. Surface water vapor mixing ratio is calculated by assuming ice-saturated conditions. The effects of leads and open water are neglected. We note that open water contributes significantly to the local turbulent fluxes of heat and moisture in the Arctic (Pinto and Curry 1995) and can therefore influence the cloud microphysics on a subgrid scale.

Aerosol properties are based on CN and CCN aircraft measurements taken during clear-sky periods in May 1998 as part of FIRE–ACE (Yum and Hudson 2001). We choose aerosol properties measured during clear-sky conditions to avoid low concentrations associated with nucleation and particle scavenging in the cloud layer and below. The aerosol number concentration, N_a, is given by observed CN concentrations, which ranged from ~350 to 700 cm^{-3} with the larger values occurring at higher altitudes. These aerosol concentrations are similar to those obtained by Radke et al. (1984) during an arctic haze event. Since detailed measurements of aerosol size and composition were lacking, we must infer values for the aerosol parameters needed by the model (i.e., size and composition) from the observed CCN activity spectra and reports in the literature. A soluble volume fraction of 75% (with the soluble portion consisting of ammonium sulfate) is specified based upon the occurrence of high sulfate aerosols in the Arctic during springtime haze events (Borys 1989). The aerosol size parameters (mode and slope of the size distribution) were found by matching calculated CCN activity spectra [using the observed number concentration and assumed composition in Eq. (14) of Part I] with observed CCN spectra obtained during the three sampling missions flown during clear-sky conditions. These values are 3.5 for the slope and 0.05 μm for the mode. Note that these aerosol characteristics were observed near the end of May; it is likely that the actual aerosol properties varied during 1 April–15 May as indicated by sun photometer measurements of aerosol optical depth (R. Stone 2004, personal communication). The impact of aerosol size, number concentration, and solubility on the cloud microphysics and radiation is examined in section 6b.

5. Baseline simulation

The SHEBA column was fairly cloudy during the time period of interest, with lidar depolarization measurements indicating that supercooled liquid water was frequently present. Mixed-phase boundary layer stratus occurred every few days in April and were present more or less continuously from 30 April to 15 May associated with a surface-based mixed layer. Mid- and upper-level cloudiness occurred when synoptic conditions favored a moist southerly flow (Wylie 2001). Higher-level clouds often occurred over the boundary layer stratus. Lower-tropospheric temperatures during 1 April to 15 May were generally between $-25°$ and $-5°$C. Surface air temperatures during much of April were unseasonably warm, although the troposphere remained below freezing during the entire period.

Overall, the modeled mean and standard deviation of the cloud-base (lowest layer) and cloud-top (highest layer) heights, layer thickness, and number of layers are fairly similar to observations (Table 1). However, the mean predicted cloud-top height (highest layer) is somewhat higher than observed and the cloud-bottom height (lowest layer) is somewhat lower than observed. These biases may be at least partially attributed to the rather coarse vertical resolution in the model, particularly above 2 km. Low vertical resolution may also explain the somewhat lower mean number of cloud layers and greater layer thickness produced by the model. The biases in predicted mean cloud-top height and layer thickness may also be attributed to uncertainty in the observed values; the observed cloud-top heights may be biased low since radar has difficulty detecting small particles near cloud top (Intrieri et al. 2002).

The predicted total cloud fraction (i.e., fraction of time clouds are present in the column) is similar to the observed value (Table 2). The observed partitioning of cloud phase indicated by liquid and ice fractions (i.e., fraction of time liquid or ice is present in the column) is generally reproduced by the model, although the liquid and ice fractions are somewhat lower and higher, respectively, than observed. The difference between the observed total and ice fractions indicates that supercooled liquid-phase clouds were present about 10% of the time. The model predicts very few liquid-phase clouds; instead, most of the supercooled water is con-

TABLE 1. Modeled and observed cloud-bottom height (lowest layer), cloud-top height (highest layer), and layer thickness (in meters) and number of layers.

	Cloud-bottom (lowest layer)	Cloud-top (highest layer)	Layer thickness	Number of layers
Modeled mean	254	4322	2427	1.16
Observed mean	399	3824	1924	1.35
Modeled std dev	1120	3040	2634	0.40
Observed std dev	1080	2719	1746	0.59

TABLE 2. Modeled and observed cloud fractions (%).

	Total fraction	Liquid fraction	Ice fraction
Modeled	82.5	49.9	82.4
Observed	85.4	64.4	74.8

tained in mixed-phase clouds. We note that it is possible that some of the clouds that were retrieved as liquid phase may have contained small amounts of ice. The modeled cloud fractions are fairly insensitive to the threshold water content (10^{-5} g m^{-3}) indicating the presence of cloud water. Even though the modeled liquid fraction is somewhat lower than observed, the predicted ratio of mean LWP and IWP of 1.22 is larger than the ratio of 0.74 for the retrievals, consistent with accurate prediction of mean LWP but underprediction of mean IWP (Table 3). These results indicate that when the model predicts supercooled liquid water, the LWP is relatively large, even though liquid occurs somewhat less frequently in the simulation than was indicated by retrievals. The modeled standard deviation of LWP is similar to the retrieved value, although the standard deviation of IWP is much smaller. Large standard deviation in the retrieved IWP may correspond with significant spatial variability in the ice hydrometeor field in mixed-phase clouds observed during FIRE–ACE (Lawson et al. 2001; Zuidema et al. 2005) that is difficult for the model to resolve.

Cloud phase partitioning is also indicated by the ratio LWP/TWP (TWP = LWP + IWP) as a function of the cloud-top temperature, T_{ct} (Fig. 1). Values of LWP/TWP < 0.4 (indicating relatively large IWP) occur at T_{ct} less than about 262 K in both the simulation and retrievals. In addition, both the modeled and retrieved ratios tend to cluster at either zero or >0.6. However, the retrievals show a number of values near unity even at temperatures colder than 250 K, while the model produces values of LWP/TWP generally between 0.6 and 0.95 at temperatures <254 K and very little liquid below 250 K. This bias may be due to an overestimation of the number of IN due to contact freezing at temperatures <254 K. The results exhibit moderate sensitivity to the number of contact IN, which is specified following Cooper (1986; see Part I): Sensitivity tests using the Fletcher (1962) or Meyers et al. (1992) formulations for the number of contact IN produce a mean LWP 27% larger and 34% smaller, respectively, compared to baseline. Low IN concentrations in the actual cloud layer may have occurred as a result of nucleation
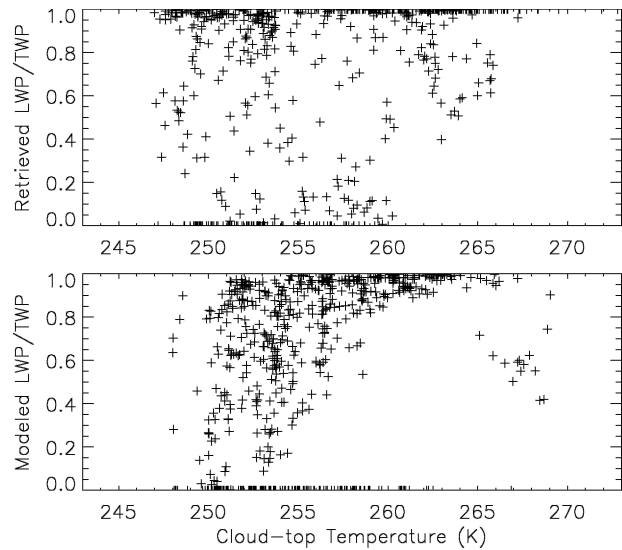

FIG. 1. Modeled and retrieved LWP/TWP (TWP = LWP + IWP) as a function of cloud-top temperature for clouds with a top height <3 km.

and particle scavenging, with the production of ice controlled by intermittent entrainment of IN into the layer (Carrio et al. 2005) if sufficient IN were available in the free atmosphere.

Time series of modeled and retrieved LWP during the period show that the predicted values of instantaneous LWP often differ substantially from retrieved values (Fig. 2). However, this is not surprising given the difficulty of correctly predicting the cloud and thermodynamic properties at given times due to errors in the initialization and forcing profiles in addition to uncertainties in the model physics. Nonetheless, qualitative features seen in the retrieved LWP time series are captured by the model, including the periodic occurrence of liquid water during 1–10 April, the presence of sig-

TABLE 3. Modeled and retrieved LWP and IWP (g m^{-2}).

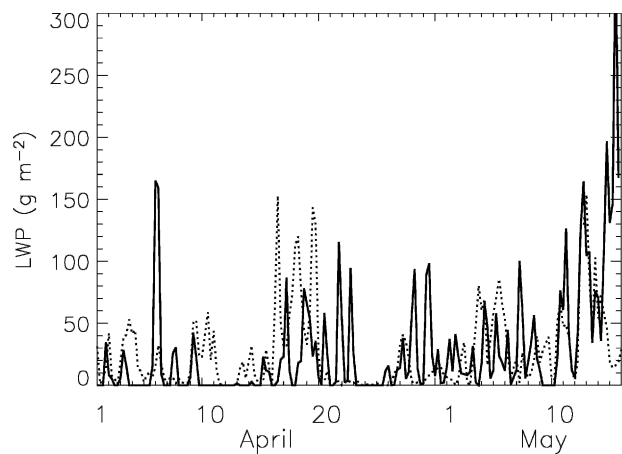|	LWP	IWP
Modeled mean	28.0	22.9
Retrieved mean	25.6	34.6
Modeled std dev	50.7	60.8
Retrieved std dev	45.4	92.1

FIG. 2. Time series of modeled (solid) and MWR-retrieved (dotted) LWP (data are 6-h averages).

nificant liquid between 15–20 April, and nearly continuous liquid water from 26 April to 15 May with the exception of 9 May. The largest values of LWP in the simulation occur during mid May with LWPs exceeding 300 g m^{-2}.

The model biases are primarily associated with low (<3 km) rather than high (>3 km) clouds as shown in Table 4. The mean IWP for high clouds is somewhat larger than retrieved, while the high-cloud ice fraction is quite close to observations. Note that the predicted high clouds are quite sensitive to the initial RH. A sensitivity simulation in which the temperature-dependent modification to the initial RH (see section 4) is neglected produces a high-cloud ice fraction of only 31%. The mean IWP in low clouds is about one-half of the retrieved value. Since low-level clouds in the Arctic primarily form as a result of air mass modification rather than large-scale forcing (Curry 1983), this bias may indicate a deficiency in the model physics. The mean modeled values of IWC in mixed-phase and low clouds (Table 5) are smaller than retrieved (particularly for mixed-phase clouds) while the predicted mean high cloud IWC is somewhat larger (the modeled and retrieved values are screened to include only ice water contents ≥ 0.5 mg m^{-3}). The mean total IWC (for IWCs ≥ 0.5 mg m^{-3}) is close to the retrieved value.

Mean surface downwelling shortwave (SW) and longwave (LW) radiative fluxes predicted by the model are somewhat higher and lower, respectively, than observed (Table 6). The mean total downwelling flux (SW plus LW) is close to observed, differing by only 1.6 W m^{-2}. The underprediction of LW flux and overprediction of SW flux are consistent with the lower simulated liquid fraction compared to retrievals. Biases in the radiative fluxes may also result from neglect of aerosol in the calculations of radiative transfer.

The predicted total precipitation accumulated at the surface during the time period (consisting almost entirely of snow) is close to observed (see Table 6). The accurate prediction of precipitation is not surprising given that it is mostly determined by the large-scale moisture convergence (Morrison and Pinto 2004), which was constrained to SHEBA observations (see section 4).

A detailed analysis of the simulation for the period 1–8 May further illustrates the model's performance. This period was characterized by a persistent low-level mixed-phase stratus that has been a focus of several observational and modeling studies (e.g., Curry et al.

TABLE 5. Modeled and retrieved mean IWC (mg m^{-3}).

	IWC (total)	IWC (mixed phase)	IWC (<3 km)	IWC (>3 km)
Modeled	12.3	10.9	13.0	8.2
Retrieved	12.4	17.3	17.0	6.4

2000; Lawson et al. 2001; Girard and Curry 2001; Dong et al. 2001; Carrio et al. 2005; Zuidema et al. 2005). Time–height plots of the modeled and retrieved IWC (Fig. 3) show that the model produces a persistent low-level stratus qualitatively similar to retrievals, although the predicted cloud top is often 500 m or more higher than retrieved. This bias may be attributed to potential deficiencies in the boundary layer parameterization, model forcing, and/or vertical resolution. The upper-level clouds indicated by retrievals on 4 and 6 May seeded the boundary layer cloud from above, leading to rapid depletion of the supercooled liquid (Curry et al. 2000; Zuidema et al. 2005). Similarly, the predicted low-level cloud is seeded by upper-level clouds on 4 May, although the cirrus predicted on 5 and 6 May does not precipitate down to the boundary layer cloud.

Time–height plots of the predicted LWC and droplet concentration and the constrained adiabatic LWC in Fig. 4 show that the predicted low-level cloud has a liquid-topped layer similar to observations. However, the predicted cloud-top height is generally 500 to 1000 m too high as was discussed above. The modeled liquid water contents also tend to be smaller than the constrained adiabatic values, although this is compensated by the greater vertical extent of the predicted liquid layer. These differences may result in part from coarse vertical resolution in the model. The simulated droplet concentration is high (>100 cm^{-3}) through most of the cloud layer, with peak values near cloud base occasionally exceeding 300 cm^{-3}. The droplet concentrations from aircraft FSSP measurements on 4 and 7 May are similar in magnitude but exhibited somewhat less variation with height (not shown). The modeled liquid layer is maintained through radiative cooling and large-scale moisture convergence, with ice generated mostly through contact freezing and subsequently precipitating below the liquid base. This canonical structure of a liquid-topped, weakly precipitating, mixed-phase stratus in both Arctic and midlatitude regimes has been described by many researchers (e.g., Rauber and Tokay 1991; Hobbs and Rangno 1998; Rangno and Hobbs 2001; Fleishauer et al. 2002; Korolev et al. 2003). Low-

TABLE 4. Modeled and observed high (>3 km) and low (<3 km) cloud fractions (%) and mean IWP (g m^{-2}).

	Low liquid fraction	Low ice fraction	Low IWP	High liquid fraction	High ice fraction	High IWP
Modeled	47.6	79.4	16.7	6.2	46.0	6.1
Observed	63.7	68.9	30.4	8.5	44.1	4.3

TABLE 6. Modeled and observed downwelling shortwave (SW), longwave (LW), and total (TOT) radiative flux (W m^{-2}) and accumulated precipitation (PREC) (cm) at the surface.

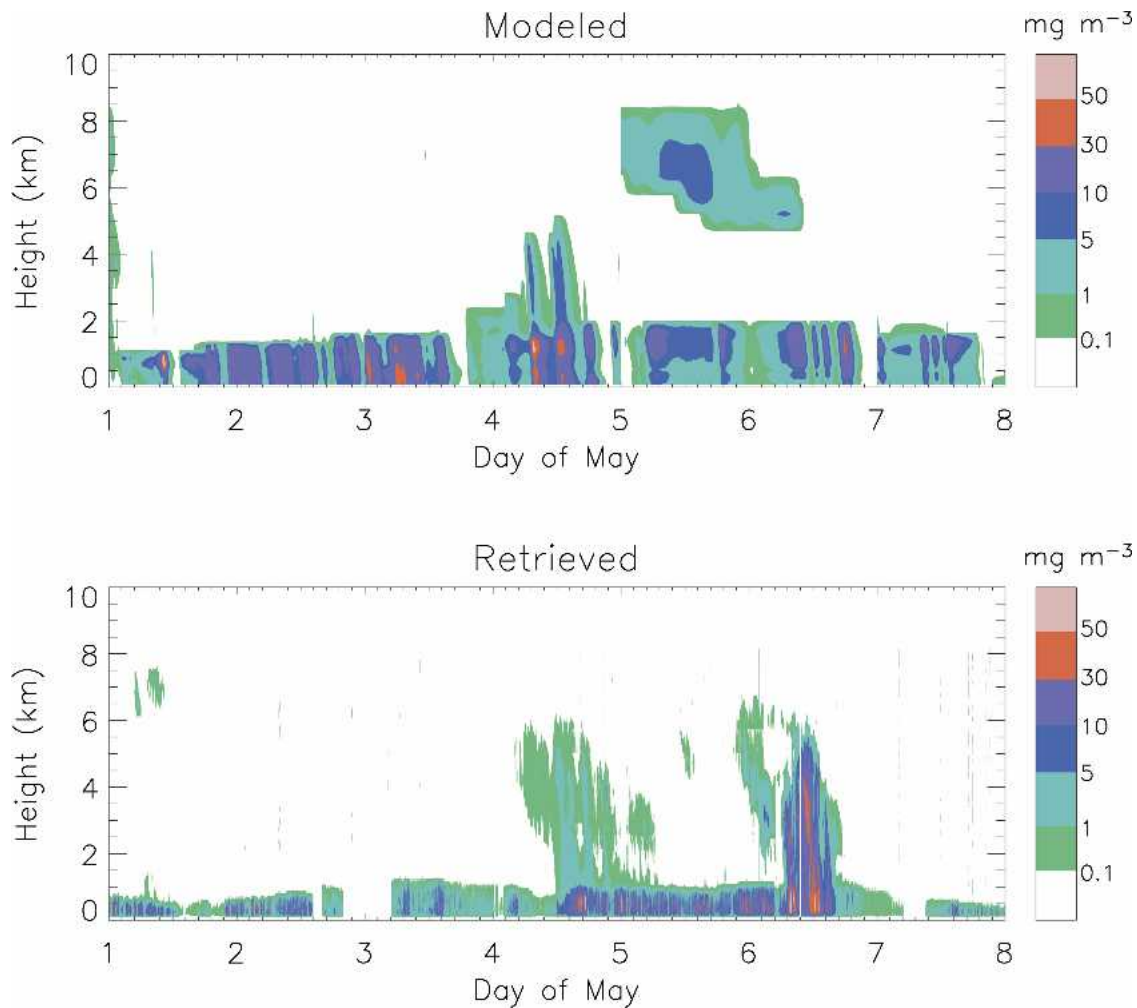|	SW	LW	TOT	PREC
Modeled	175.1	216.9	392.0	2.24
Observed	165.1	225.3	390.4	2.16

FIG. 3. Modeled and retrieved ice water contents for the period 1–8 May.

level mixed-phase stratus during other time periods of the simulation exhibit a similar structure.

The mean modeled droplet concentration of 180 cm^{-3} during the period 1–8 May is somewhat smaller than the mean value obtained with aircraft FSSP of 222 cm^{-3} (both the modeled and observed values were screened to include only droplet concentrations exceeding 50 cm^{-3}). The modeled layer-mean droplet effective radius of 5.4 μm is slightly larger than the value of 4.4 μm calculated by applying the mean FSSP droplet concentration to the constrained adiabatic LWC profiles as described in section 2. The predicted subgrid-scale vertical velocity is similar to observations of standard deviation vertical velocity in arctic mixed-phase stratus (Pinto 1998), with values ranging from 0.1 to 0.35 m s^{-1}. A sensitivity test in which subgrid vertical velocity is neglected produces a substantially smaller droplet number concentration and mean effective radius of 10.5 μm during 1–8 May. These results highlight the importance of subgrid vertical motion when param-

eterizing droplet nucleation in large-scale models, which was also described by Ghan et al. (1997). The predicted droplet concentration exhibits only a small sensitivity to the vertical resolution. Doubling the vertical resolution in the lowest ~2 km decreases the mean droplet concentration during 1–8 May by only 5%. Similarly, the number concentration exhibits little sensitivity to the time step; a reduction of the time step to 1 min increases the mean droplet concentration by 7%.

The predicted ice particle number concentrations (a few per liter) during 1–8 May are much smaller than aircraft observations on 4 May (hundreds per liter) reported by Lawson et al. (2001). For a given IWC, a large number of small crystals uptake water vapor faster than smaller numbers of large crystals due to differences in the crystal surface area density. Thus, large ice number concentrations lead to an enhanced Bergeron–Findeisen process that would be expected to rapidly glaciate the mixed-phase cloud. The coexistence of supercooled liquid water and high crystal concentra-
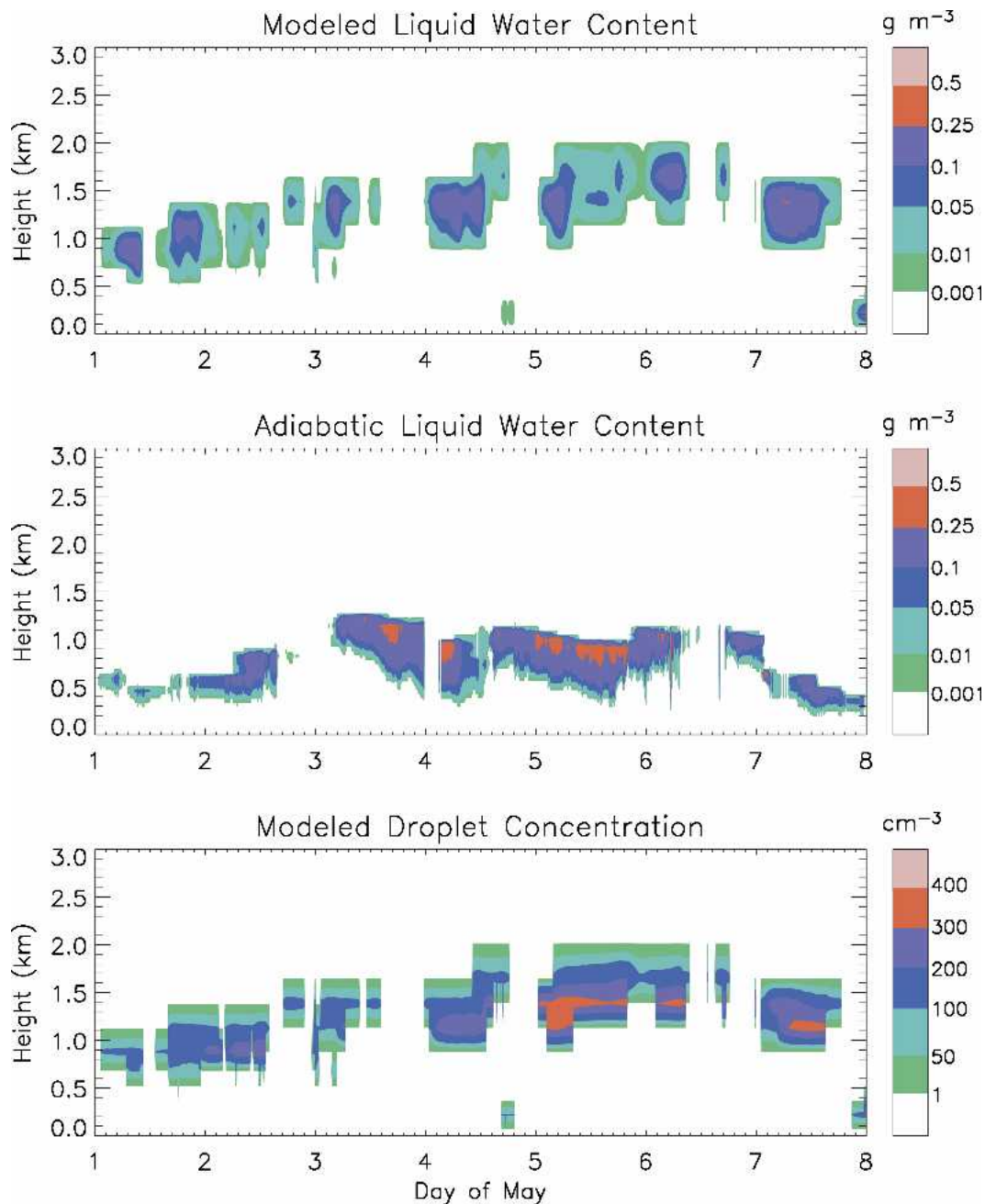
FIG. 4. Modeled liquid water content and droplet number concentration and MWR-constrained adiabatic liquid water content using lidar-derived cloud base for the period 1–8 May.

tions can perhaps be explained by ice particles that were present in localized pockets instead of occurring throughout the cloud layer (Fu and Hollars 2004). That stated, the observations are uncertain and highly variable in space and time. The modeled ice crystal concentration is not particularly sensitive to the vertical resolution and time step during 1–8 May since ice is formed mostly as a result of droplet freezing. However, during other times when aerosol freezing is the domi-

nant production mechanism (particularly for upper-level clouds), the crystal concentration is much more sensitive to the time step.

6. Sensitivity experiments

a. Microphysics parameterization

Three different microphysics parameterizations are incorporated into the ARCSCM to simulate the

1 April–15 May period of SHEBA. These results are compared with the baseline simulation (hereafter referred to as BASE) to further interpret its performance. The three parameterizations are briefly described below in order of increasing complexity. Values of relevant microphysical parameters (e.g., fall speeds, particle densities) are specified to be the same for the various schemes.

The first parameterization is a version of the Reisner et al. (1998) single-moment bulk scheme that predicts the mixing ratios of droplets, cloud ice, rain, and snow (hereafter SM) and is capable of simulating mixed-phase clouds. The mixing ratio of each species is prognosed at a given level allowing for more realistic phase partitioning than provided by simple temperature–phase relationships. This scheme has been used extensively for simulations of Arctic climate (Pinto et al. 1999; Curry et al. 2000; Girard and Curry 2001; Morrison et al. 2003). The cloud ice number concentration is specified following Cooper (1986) as a function of the temperature. Droplet and cloud ice populations are assumed to be monodisperse. Cloud–aerosol interactions are neglected; droplet effective radius is assumed to be 5 μm.

The second scheme combines the detailed ice-phase parameterization of the BASE parameterization with the simple liquid-phase microphysics of SM (hereafter DI). Thus, the DI scheme prognoses the number concentrations of cloud ice and snow in addition to the mixing ratios of the four hydrometeor species (droplets, cloud ice, rain, snow). The production of ice from freezing of aerosol is included, while droplet activation of aerosol is neglected.

The third parameterization includes the ice-phase and liquid-phase parameterizations of the BASE scheme but also predicts the mixing ratio and number concentration of graupel (hereafter GR). The graupel parameterization follows that described by Reisner et al. (1998), Murakami (1990), and Ikawa and Saito (1991).

The addition of graupel microphysics increases the mean LWP while decreasing the mean IWP only slightly (Table 7). Liquid and ice fractions are similar between the BASE and GR simulations. Time series of LWP difference (GR − BASE) show the most significant differences in mid May (Fig. 5) when liquid water paths are large. The incorporation of graupel increases
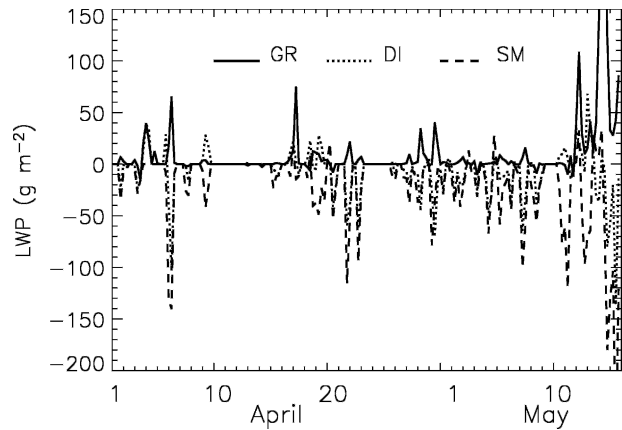

FIG. 5. LWP differences (sensitivity minus baseline) using the three different microphysics schemes.

the mean fall speed of precipitating ice since the fall speed of graupel is much higher than that of snow for same-sized particles. This reduces the amount of precipitation ice in the column relative to BASE, resulting in less accretion of droplets and a reduced Bergeron–Findeisen process. The model exhibits similar sensitivity to increased snowfall velocity.

Mean LWP and IWP are smaller and larger, respectively, using the DI scheme compared to BASE (see Table 7). The time series of LWP difference (see Fig. 5) reveals significant differences in the LWP for a given time. Liquid water paths are generally larger than BASE between 10 and 20 April when cloud temperatures were relatively warm and are smaller during 26 April–8 May when temperatures were colder. Differences in the LWP between the simulations are mostly the result of differences in the parameterization of droplet freezing. The BASE scheme includes separate contributions from contact and immersion freezing as a function of droplet size that varies in time and space (see Part I) while the DI scheme calculates droplet freezing using a constant droplet size.

The SM scheme produces a much smaller mean LWP and liquid fraction compared to BASE and retrievals (see Table 7). Time series of LWP difference also reveal much smaller liquid water paths produced by the SM scheme relative to BASE. However, the ice fraction is somewhat higher than BASE and retrievals. These

TABLE 7. Observed/retrieved (OBS) and modeled mean LWP, IWP (g m^{-2}), LW and SW radiative fluxes at the surface (W m^{-2}), liquid, ice, and total cloud fractions (%), and run time relative to BASE (%) using the different microphysics parameterizations.

	LWP	IWP	Liquid fraction	Ice fraction	Total fraction	LW	SW	Run time
BASE	28.0	22.9	49.9	82.4	82.5	216.9	175.1	100.0
GR	38.5	22.0	51.3	82.3	82.9	218.2	170.0	103.5
DI	21.9	23.9	49.6	81.2	81.4	214.9	176.8	93.4
SM	8.3	21.9	19.5	89.9	89.9	205.2	195.7	91.5
OBS	25.6	34.6	64.4	74.8	85.4	225.3	165.1	NA

TABLE 8. Observed/retrieved (OBS) and modeled mean LWP, IWP (g m^{-2}), liquid and ice fractions (%), mean droplet effective radius (r_e) (μm), number concentration (N_c) (cm^{-3}), percent of aerosol activated as droplets, and downwelling longwave and shortwave radiative fluxes at the surface (W m^{-2}), for the various aerosol properties indicated; N_c are r_e are calculated by screening for values of droplet concentration >50 cm^{-3} and cloud water mixing ratio >0.001 g m^{-3}, respectively.

	LWP	IWP	Liquid fraction	Ice fraction	r_e	N_c	Percent activated	LW	SW
$r_{min} = 0.1$ μm	29.2	25.6	49.6	82.6	4.7	338	79.7	218.5	167.2
$r_{min} = 0.02$ μm	21.7	23.3	54.1	82.0	8.4	83	20.0	218.5	181.6
Sol. = 50%	20.7	24.4	27.7	80.9	7.1	135	33.7	207.3	191.0
Sol. = 100%	31.6	24.7	61.8	84.4	5.4	182	42.2	223.5	164.9
N_a = base/2	27.0	24.8	50.3	83.7	6.8	107	50.8	217.9	176.6
N_a = base $\times$ 3	27.9	25.6	47.1	81.7	4.9	303	23.8	216.9	172.0
BASE	28.0	22.9	49.9	82.4	6.0	156	36.7	216.9	175.1
OBS	25.6	34.6	64.4	74.8	—	—	—	225.3	165.1

results suggest incorrect phase partitioning in the SM scheme, that is, mixed-phase clouds are often predicted as entirely crystalline. The large differences in cloud phase and mean LWP result in differences in the mean downwelling LW and SW fluxes at the surface of -11.7 and 20.2 W m^{-2}, respectively, compared to BASE and even larger biases relative to observations. These biases are consistent with previous results using the scheme to simulate mixed-phase stratus (Curry et al. 2000; Girard and Curry 2001; Morrison et al. 2003). As described by Morrison et al. (2003), the SM scheme is highly sensitive to the specified crystal concentration since it determines in part the uptake of water vapor by crystals. Incorporating the Fletcher (1962) or Meyers et al. (1992) formulations produces a mean LWP of 16.6 and 1.1 g m^{-2}, respectively. This sensitivity highlights the importance of realistically treating the ice number concentration.

A limitation of using the Meyers et al., Fletcher, Cooper, and similar formulations to parameterize the ice number concentration is that these expressions are generally functions of either temperature or supersaturation. Extensions of classical nucleation theory (Khvorostyanov and Sassen 1998; Khvorostyanov and Curry 2000) suggest both a temperature and supersaturation dependence for the number of IN occurring through homogeneous or heterogeneous freezing. Empirical formulations can also produce unrealistic values when extrapolated to cold temperatures ($<\sim-30°C$) and therefore must be arbitrarily modified (e.g., Reisner et al. 1998). In addition, sedimentation of ice into drier layers or a rapid decrease in supersaturation after nucleation can result in high crystal concentrations at low supersaturations that cannot be predicted if the crystal concentration is diagnosed rather than prognosed. For example, initially large values of supersaturation can produce an impulse of nucleation and high crystal concentration, but the supersaturation decreases rapidly owing to vapor deposition onto the crystals. Diagnosing the ice number concentration from supersaturation in this instance will result in an underprediction of concentration after the supersaturation decreases.

An important consideration for any model parameterization is its computational cost. The cost associated with each microphysics scheme is estimated by comparing run times for the various simulations (see Table 7). While this estimate cannot provide an exact cost for each scheme since other parameterizations in the model also contribute to run time, it is useful for comparing relative differences in efficiency between the schemes. As expected, run times increase with increasing complexity of the microphysics parameterization, varying by $\sim$15% using the four different schemes. Incorporating the detailed ice-phase microphysics into the SM scheme increases the run time by only a few percent for the DI scheme; using BASE increases the cost $\sim$10% relative to SM, while adding graupel microphysics to BASE increases the run time by a few percent for the GR scheme. Another issue that must be considered in certain applications is memory allocation as the number of prognostic variables is increased. The number of prognostic variables ranges from 4 in SM to 10 in GR.

b. Aerosol characteristics

Since aerosol and cloud microphysics are closely coupled in the new scheme, the specified aerosol properties play an important role in the evolution of the predicted clouds. To assess this role, we conduct sensitivity simulations of the 1 April–15 May period varying the aerosol size, solubility, and number concentration. Results are shown in Table 8. Note that other aerosol parameters can impact the nucleating ability of the particles [i.e., wettability, relative area of active sites, misfit strain parameter; see Khvorostyanov and Curry (2000)] but are not tested here.

The sensitivity to changes in aerosol size is examined by performing simulations with an aerosol modal radius (r_{min}) of 0.1 and 0.02 μm, compared to the baseline value of 0.05 μm. A distribution of larger aerosol increases the number of CCN since larger aerosols preferentially activate. Thus, the droplet number concentration is increased (decreased) and effective radius decreased (increased) as the aerosol size increases (decreases). The smaller (larger) droplets freeze less (more) efficiently since contact and immersion freezing

are functions of droplet size, producing larger (smaller) LWPs. Interestingly, when the droplet size is increased due to smaller specified aerosol (implying faster contact/immersion freezing rates and increased precipitation efficiency), the average mixed-phase cloud lifetime (indicated by the liquid fraction) actually increases. This occurs because the number of IN is reduced due to decreasing ice nucleability associated with the smaller aerosol (i.e., less surface area is available to form a substrate for the ice crystal). With fewer crystals available, the Bergeron–Findeisen mechanism is less effective, leading to the persistence of liquid water in the simulation. The mean LW and SW surface radiative fluxes reflect these results. The increase (decrease) in downwelling surface SW flux is consistent with a decrease (increase) in the cloud albedo associated with larger (smaller) droplet effective radius and smaller (larger) mean LWP. This indirect aerosol effect has been described in numerous studies (e.g., Twomey 1977; Ghan et al. 2001; Penner and Rotstayn 2001; Feingold et al. 2003). The LW flux responds more to changes in the mixed-phase cloud lifetime. Relative to baseline, the mean surface downwelling LW flux increases with decreasing aerosol size due to the increased mixed-phase cloud lifetime even though mean LWP is decreased 23%. This occurs because the predicted clouds tend to emit as blackbodies in both the baseline and sensitivity simulations.

The sensitivity of the model to changes in aerosol solubility is examined by performing simulations with a soluble fraction of 100% and 50% compared to 75% for the baseline value. Specifying a soluble fraction of 100% implies no condensation freezing of aerosol in the model (contact and immersion freezing of droplets are still allowed). The solubility of an aerosol population depends on its source and may change over time. For example, solubility increases if sulfate loading of the aerosol occurs in a polluted air mass (Pruppacher and Klett 1997). Seasonal changes in solubility may coincide with the presence of arctic pollution haze in the spring and early summer (e.g., Borys 1989; Curry 1995; Curry et al. 1996). The mean droplet number concentration and effective radius exhibit moderate sensitivity to soluble fraction while the average mixed-phase cloud lifetime exhibits large sensitivity. Decreasing solubility leads to increased ice nucleability and shorter mixed-phase lifetimes. Even though solubility also influences the droplet effective radius, this effect is relatively minor; the response of the SW and LW radiative fluxes is dominated by changes in the mixed-phase cloud lifetime. Decreased (increased) mixed-phase cloud lifetime due to decreased (increased) aerosol solubility leads to increased (decreased) SW and decreased (increased) LW downwelling fluxes at the surface. Thus, a mixed-phase cloud lifetime SW and LW radiative indirect aerosol effect due to modification of aerosol solubility is identified. Note that specifying a soluble fraction of 100% produces results that are quite similar to observations for a number of quantities.

Changes in the aerosol number concentration are expected to impact the number of IN and CCN. Aerosol number concentration varies widely between air masses originating in different source regions (e.g., continental versus marine). Anthropogenic aerosol can significantly modify the total aerosol concentration; in urban environments, the aerosol concentration is often several orders of magnitude larger than in pristine conditions (Pruppacher and Klett 1997). The sensitivity of the model to aerosol number concentration is assessed by performing simulations with concentrations of aerosol specified at three times and one-half times the baseline values described in section 4. Increasing (decreasing) the aerosol number concentration increases (decreases) the mean droplet number and decreases (increases) the effective radius as expected. The downwelling SW flux at the surface is influenced by changes in droplet effective radius as the aerosol number concentration is modified. The LW flux exhibits little sensitivity since the mixed-phase cloud lifetimes vary only slightly in response to changes in the aerosol number concentration.

These results suggest that the SW indirect aerosol radiative effect operates through distinct mechanisms (droplet size, LWP, and cloud lifetime effects), which is consistent with previous studies. However, the cloud lifetime effect appears to differ in arctic mixed-phase stratus compared to liquid-phase clouds, which have been studied much more extensively. As opposed to liquid-phase clouds, the lifetime of arctic mixed-phase stratus appears to be strongly linked to the ice nucleability of the aerosol rather than the droplet size or number concentration. For example, modification of aerosol resulting in more numerous and smaller droplets, which tends to increase the lifetime of liquid-phase clouds (e.g., Albrecht 1989), may actually decrease the lifetime of mixed-phase clouds if the IN concentration also increases. This mixed-phase cloud lifetime effect on the downwelling SW flux is particularly evident for changes in the aerosol solubility. These results also suggest a LW indirect aerosol radiative effect (cloud greenhouse effect), which is mostly determined by changes in the mixed-phase cloud lifetime. Indirect aerosol effects on the LW flux have not been extensively studied, but may be particularly important in the Arctic where the LW flux dominates the solar flux during most of the year.

This study provides a link between the chemical and physical properties of the aerosol and previous studies suggesting that the maintenance of mixed-phase stratus is dependent upon the IN concentration (Pinto 1998; Harrington et al. 1999; Jiang et al. 2000; Morrison et al. 2003). A similar IN cloud lifetime–radiative effect associated with contact freezing of droplets was described by Lohmann (2002) but did not explicitly relate cloud lifetime to aerosol properties in terms of condensation

freezing on aerosol. Inclusion of aerosol–IN interactions associated with contact and immersion freezing of droplets in the model (an area of future development) would likely enhance the IN cloud lifetime effect described here.

7. Summary and conclusions

A single-column model incorporating the new microphysics scheme described in Part I was used to simulate the 1 April–15 May period of SHEBA. Results were compared to observations and ground-based retrievals. The model was initialized with SHEBA observations and forced with constrained ECMWF model output. Aerosol properties needed by the microphysics scheme were based on aircraft measurements taken during FIRE–ACE. Simulations were reinitialized every three days to limit model drift in the temperature and water vapor profiles.

The model was able to reasonably predict the mean cloud properties observed during the period. Cloud boundaries and total fraction were similar to observations. Phase partitioning in the simulation, crucial for predicting the surface radiative fluxes, was fairly similar to retrievals as indicated by liquid and ice fractions and ratios of LWP and total water path as a function of cloud-top temperature. However, the predicted liquid fraction was somewhat lower than retrieved and the model produced relatively less liquid water than indicated by retrievals in strongly supercooled clouds with a cloud-top temperature <254 K. Mean LWP was close to the retrieved value while mean IWP was somewhat smaller than retrieved. Biases in the predicted downwelling surface solar and longwave radiative fluxes were consistent with the small underprediction of liquid cloud fraction. Neglect of aerosol in the radiative transfer calculations may have also contributed to biases in the radiative fluxes.

A detailed evaluation of the simulation for the period 1–8 May showed that the model was able to qualitatively reproduce many features of a persistent mixed-phase boundary layer stratus. However, the predicted cloud top was generally too high by about 500–1000 m, indicating potential deficiencies associated with the boundary layer parameterization, large-scale forcing, and/or coarse vertical resolution. Improvements in these areas may be needed to fully benefit from improvements in the new microphysics scheme. In addition, the modeled ice phase microphysics differed widely from in situ observations. However, the in situ and retrieved ice microphysical properties are uncertain; a better characterization is needed, particularly regarding the ice particle number concentration.

Parallel simulations using three different microphysics parameterizations were compared to further assess the new scheme. The simple liquid/detailed ice and graupel microphysics schemes produced mean LWPs that were smaller and larger than baseline, respectively. Mean IWP and liquid and ice fractions did not vary significantly from baseline using either scheme. The single-moment scheme produced only a small amount of liquid water resulting in significant differences in the downwelling surface radiative fluxes compared with observations, consistent with previous studies (Curry et al. 2000; Girard and Curry 2001; Morrison et al. 2003). This bias was mostly attributed to uncertainties in the diagnosed ice number concentration. These results suggest the importance of realistically treating the crystal concentration. We argue that prognosing, rather than diagnosing, the crystal concentration is needed for a realistic treatment of the ice microphysics. Computational time increased somewhat (~10%–13%) using the more complex schemes, although the number of prognostic variables (ranging from 4 in SM to 10 in GR) may be important if memory allocation is an issue in the model. Of course, a drawback in using the simpler schemes (DI and SM) is that cloud–aerosol interactions are not explicitly treated for both liquid and ice, limiting their ability to model indirect aerosol effects on climate.

The sensitivity of the model to modification of the specified aerosol was assessed. The response was determined by two effects: 1) changes in the ice nucleability and thus IN concentration and 2) changes in CCN concentration. Changes in IN concentration had a large influence on the lifetime of mixed-phase clouds while modification of CCN affected droplet number concentration and effective radius. The response of the surface radiative fluxes was determined by the interplay between these two effects. The downwelling shortwave flux responded to changes in the cloud albedo as a function of the droplet effective radius. The longwave flux was mostly influenced by changes in the lifetime of mixed-phase clouds. The surface radiative fluxes (both shortwave and longwave) exhibited particular sensitivity to changes in the aerosol solubility mostly due to the mixed-phase cloud lifetime effect. We note, of course, that the simulated response of clouds and radiation to modification of aerosol is uncertain owing to an incomplete treatment of the aerosol and cloud microphysics and other physical processes, deficiencies in the initialization and forcing, and coarse resolution (exhibited by biases in the clouds and radiation in the baseline simulation); nonetheless, these results suggest qualitatively that aerosol indirect effects in arctic mixed-phase clouds are complex and merit further study.

This work represents a first step in evaluating the microphysics scheme. We note that there were uncertainties in the advective forcing, initialization profiles, specified aerosol properties, neglect of horizontal cloud water advection, etc. In addition, other model parameterizations (e.g., radiation, boundary layer schemes) can contribute to biases in the predicted cloud properties. Hence, this study cannot provide an unambiguous evaluation of the microphysics parameterization. More

rigorous testing is needed including incorporation into 3D models and application to regions outside of the Arctic. Model results were particularly sensitive to the aerosol size, concentration, and composition, which are not well known in the Arctic owing to limited observations. This paper underlines the need for better characterization of aerosols in the region, including the development of a detailed aerosol climatology for the central Arctic.

We did not discuss at length how the model resolution can affect results. Since the microphysics scheme predicts clouds based on grid-scale values of relative humidity (i.e., there is no subgrid-scale cloud parameterization), we implicitly assumed that clouds at SHEBA could be captured using the given resolution. While clouds that occurred at SHEBA were predominately stratiform and horizontally extensive, they often occurred in vertically thin layers. Thus, it is likely that some of these clouds were subgrid in the vertical, which may have contributed to model bias. We note, however, that it is difficult to test the model's overall sensitivity to the vertical resolution since the vertical resolution of the specified advective forcing, which is important in driving the initial formation of cloud water, cannot be increased. Incorporating the scheme into a 3D model can help to rectify this issue. Another issue that arises is the difference in horizontal scale between the model ($\sim$60 km based on the scale of the advective forcing and vertical velocity) and observations (measured at a single location). This difference likely accounted for the larger variability in the retrieved cloud properties (e.g., IWP), but was probably less important in comparisons of the time-averaged cloud properties. Nonetheless, the spatial scale of the model is important in determining appropriate values of resolution-dependent parameters in the microphysics scheme, which can influence the time-averaged cloud properties (Fowler et al. 1996). Further study is needed to better understand the role of spatial scale and subgrid cloudiness in predicting arctic clouds using a large-scale model.

Specified microphysical parameters in the new scheme play an important role in simulating arctic clouds. In particular, the ice parameters (e.g., bulk density, fall speed, habit, spectral dispersion, collection efficiency) are important in calculating several microphysical processes; yet appropriate values for these parameters remain uncertain, particularly for arctic clouds. A detailed assessment of the role of the specified microphysics parameters was beyond the scope of this paper, but should be addressed in future work.

REFERENCES.

Albrecht, B. A., 1989: Aerosols, cloud microphysics and fractional cloudiness. *Science,* **237,** 1020–1022.

Beesley, J. A., C. S. Bretherton, C. Jakob, E. L Andreas, J. M. Intrieri, and T. A. Uttal, 2000: A comparison of cloud and boundary layer variables in the ECMWF forecast model with observations at the Surface Heat Budget of the Arctic Ocean (SHEBA) ice camp. *J. Geophys. Res.,* **105,** 12 337–12 349.

Borys, R. D., 1989: Studies of ice nucleation by arctic aerosol on AGASP-II. *J. Atmos. Chem.,* **9,** 169–185.

Briegleb, B. P., 1992: Delta-Eddington approximation for solar radiation in the NCAR Community Climate Model. *J. Geophys. Res.,* **97,** 7603–7612.

Carrio, G. G., H. Jiang, and W. R. Cotton, 2005: Impact of aerosol intrusions on the Arctic boundary layer clouds. Part I: 4 May 1998 case. *J. Atmos. Sci.,* in press.

Cooper, W. A., 1986: Ice initiation in natural clouds. *Precipitation Enhancement—A Scientific Challenge, Meteor. Monogr.,* No. 43, Amer. Meteor. Soc., 29–32.

Curry, J. A., 1983: On the formation of polar continental air. *J. Atmos. Sci.,* **40,** 2279–2292.

——, 1995: Interactions among aerosols, clouds, and climate of the Arctic Ocean. *Sci. Total Environ.,* **160,** 777–791.

——, and G. F. Herman, 1985: Relationships between large-scale heat and moisture budgets and the occurrence of Arctic stratus clouds. *Mon. Wea. Rev.,* **113,** 1441–1457.

——, and E. E. Ebert, 1990: Sensitivity of the thickness of arctic sea ice to the optical properties of clouds. *Ann. Glaciol.,* **14,** 43–46.

——, W. B. Rossow, and J. L. Schramm, 1996: Overview of Arctic cloud and radiation properties. *J. Climate,* **9,** 1731–1764.

——, and Coauthors, 2000: FIRE Arctic Clouds Experiment. *Bull. Amer. Meteor. Soc.,* **81,** 5–29.

Dong, X., G. G. Mace, P. Minnis, and D. F. Young, 2001: Arctic stratus cloud properties and their effect on the surface radiation budget: Selected cases from FIRE ACE. *J. Geophys. Res.,* **106,** 15 297–15 312.

Ebert, E. E., and J. A. Curry, 1992: A parameterization of ice-cloud optical properties for climate models. *J. Geophys. Res.,* **97,** 3831–3836.

Feingold, G., W. L. Eberhard, D. E. Veron, and M. Prevedi, 2003: First measurements of the Twomey indirect effect using ground-based remote sensors. *Geophys. Res. Lett.,* **30,** 1287, doi:10.1029/2002GL016633.

Fleishauer, R. P., V. E. Larson, and T. H. Vonder Haar, 2002: Observed microphysical structure of midlevel, mixed-phase clouds. *J. Atmos. Sci.,* **59,** 1779–1804.

Fletcher, N. H., 1962: *The Physics of Rainclouds.* Cambridge University Press, 386 pp.

Fowler, L. D., D. A. Randall, and S. A. Rutledge, 1996: Liquid and ice microphysics in the CSU General Circulation Model. Part 1: Model description and simulated microphysical processes. *J. Climate,* **9,** 489–529.

Fu, Q., and S. Hollars, 2004: Testing mixed-phase cloud water vapor parameterizations with SHEBA/FIRE ACE observations. *J. Atmos. Sci.,* **61,** 2083–2091.

Ghan, S. J., L. R. Leung, and R. C. Easter, 1997: Prediction of cloud droplet number in a general circulation model. *J. Geophys. Res.,* **102,** 21 777–21 794.

——, and Coauthors, 2001: A physically-based estimate of radiative forcing by anthropogenic sulfate aerosol. *J. Geophys. Res.,* **106,** 5279–5293.

Girard, E., and J. A. Curry, 2001: Simulation of Arctic low-level clouds observed during the FIRE Arctic Clouds Experiment using a new bulk microphysics scheme. *J. Geophys. Res.,* **106,** 15 139–15 154.

Grell, G. A., J. Dudhia, and D. R. Stauffer, 1995: A description of the Fifth-Generation Penn State/NCAR Mesoscale Model (MM5). NCAR Tech. Note NCAR/TN-398+STR, 138 pp.

Harrington, J. Y., T. Reisen, W. R. Cotton, and S. M. Kreiden-weis, 1999: Cloud resolving simulations of Arctic stratus: Part II: Transition-season clouds. *Atmos. Res.,* **51,** 45–75.

Hobbs, P. V., and A. L. Rangno, 1985: Ice particle concentrations in clouds. *J. Atmos. Sci.,* **42,** 2523–2549.

——, and ——, 1990: Rapid development of ice particle concentrations in small polar maritime clouds. *J. Atmos. Sci.,* **47,** 2710–2722.

——, and ——, 1998: Microstructures of low and middle-level clouds over the Beaufort Sea. *Quart. J. Roy. Meteor. Soc.,* **124,** 2035–2071.

Holtslag, A. M., and B. A. Boville, 1993: Local versus non-local boundary-layer diffusion in a global climate model. *J. Climate,* **6,** 1825–1842.

Ikawa, M., and K. Saito, 1991: Description of the nonhydrostatic model developed at the forecast research department of the MRI. Meteorological Institute Tech. Rep. 28, 238 pp.

Intrieri, J. M., M. D. Shupe, T. Uttal, and B. J. McCarty, 2002: An annual cycle of Arctic cloud characteristics observed by radar and lidar at SHEBA. *J. Geophys. Res.,* **107,** 8030, doi:10.1029/2000JC000423.

Jiang, H., W. R. Cotton, J. O. Pinto, J. A. Curry, and M. J. Weisbluth, 2000: Cloud resolving simulations of mixed-phase arctic stratus observed during BASE: Sensitivity to concentration of ice crystals and large-scale heat and moisture advection. *J. Atmos. Sci.,* **57,** 2105–2117.

Khvorostyanov, V. I., and K. Sassen, 1998: Cirrus cloud simulation using explicit micropohysics and radiation. Part 1: Model description. *J. Atmos. Sci.,* **55,** 1808–1821.

——, and J. A. Curry, 2000: A new theory of heterogeneous ice nucleation for application in cloud and climate models. *Geophys. Res. Lett.,* **27,** 4081–4084.

Korolev, A. V., G. A. Isaac, S. G. Cober, J. W. Strapp, and J. Hallett, 2003: Microphysical characterization of mixed-phase clouds. *Quart. J. Roy. Meteor. Soc.,* **129,** 39–65.

Lawson, R. P., B. A. Baker, C. G. Schmitt, and T. L. Jensen, 2001: An overview of microphysical properties of Arctic clouds observed in May and July during FIRE ACE. *J. Geophys. Res.,* **106,** 14 989–15 014.

Lohmann, U., 2002: A glaciation indirect effect caused by soot aerosols. *Geophys. Res. Lett.,* **29,** 1052, doi:10.1029/2001GL014357.

——, J. Humble, W. R. Leaitch, G. A. Isaac, and I. Gultepe, 2001: Simulation of ice clouds during FIRE ACE using the CCCMA single-column model. *J. Geophys. Res.,* **106,** 15 123–15 138.

Lynch, A. H., W. L. Chapman, J. E. Walsh, and G. Weller, 1995: Development of a regional climate model of the western Arctic. *J. Climate,* **8,** 1555–1570.

Meyers, M. P., P. J. DeMott, and W. R. Cotton, 1992: New primary ice nucleation parameterization in an explicit model. *J. Appl. Meteor.,* **31,** 708–721.

Mlawer, E. J., S. J. Taubman, P. D. Brown, M. J. Iacono, and S. A. Clough, 1997: Radiative transfer for inhomogeneous atmospheres: RRTM a validated correlated-k model for the longwave. *J. Geophys. Res.,* **102,** 16 663–16 682.

Morrison, H., and J. O. Pinto, 2004: A new approach for obtaining advection profiles: Application to the SHEBA column. *Mon. Wea. Rev.,* **132,** 687–702.

——, M. D. Shupe, and J. A. Curry, 2003: Modeling clouds observed at SHEBA using a bulk parameterization implemented into a single-column model. *J. Geophys. Res.,* **108,** 4255, doi:10.1029/2002JD002229.

——, J. A. Curry, and V. I. Khvorostyanov, 2005: A new double-moment microphysics scheme for application in cloud and climate models. Part 1: Description. *J. Atmos. Sci.,* **62,** 1665–1677.

Murakami, M., 1990: Numerical modeling of the dynamical and microphysical evolution of an isolated convective cloud—The 19 July 1981 CCOPE cloud. *J. Meteor. Soc. Japan,* **68,** 107–128.

Ohtake, T., 1993: Freezing points of H_2SO_4 aqueous solutions and formation of stratospheric ice clouds. *Tellus,* **45B,** 138–144.

Penner, J. E., and L. D. Rotstayn, 2001: Indirect aerosol forcing, quasi forcing, and climate response. *J. Climate,* **14,** 2960–2975.

Persson, P. O. G., C. W. Fairall, E. L Andreas, P. S. Guest, and D. K. Perovich, 2002: Measurements near the Atmospheric Surface Flux Group tower at SHEBA: Near-surface conditions and surface energy budget. *J. Geophys. Res.,* **107,** 8045, doi:10.1029/2000JC000705.

Pinto, J. O., 1998: Autumnal mixed-phase cloudy boundary layers in the Arctic. *J. Atmos. Sci.,* **55,** 2016–2038.

——, and J. A. Curry, 1995: Atmospheric convective plumes emanating from leads. 2, Microphysical and radiative processes. *J. Geophys. Res.,* **100,** 4633–4642.

——, ——, and A. H. Lynch, 1999: Modeling cloud and radiation for the November 1997 period of SHEBA using a column climate model. *J. Geophys. Res.,* **104,** 6661–6678.

Pruppacher, H. R., and J. D. Klett, 1997: *Microphysics of Clouds and Precipitation.* Kluwer Academic, 954 pp.

Radke, L. F., J. F. Lyons, D. A. Hegg, and P. V. Hobbs, 1984: Airborne observations of arctic aerosols. Characterizations of arctic haze. *Geophys. Res. Lett.,* **11,** 393–396.

Randall, D. A., and D. G. Cripe, 1999: Alternative methods for specification of observed forcing in single-column models. *J. Geophys. Res.,* **104,** 24 527–24 546.

——, K.-M. Xu, R. J. C. Somerville, and S. Iacobellis, 1996: Single-column models and cloud ensemble models as links between observations and climate models. *J. Climate,* **9,** 1683–1697.

Rangno, A. L., and P. V. Hobbs, 1991: Ice particle concentrations and precipitation development in small polar maritime clouds. *Quart. J. Roy. Meteor. Soc.,* **117,** 207–241.

——, and ——, 2001: Ice particles in stratiform clouds in the Arctic and possible mechanisms for the production of high ice particle concentrations. *J. Geophys. Res.,* **106,** 15 065–15 075.

Rauber, R. M., and A. Tokay, 1991: An explanation for the existence of supercooled water at the top of cold clouds. *J. Atmos. Sci.,* **48,** 1005–1023.

Reisner, J., R. M. Rasmussen, and R. T. Bruintjes, 1998: Explicit forecasting of supercooled liquid water in winter storms using the MM5 forecast model. *Quart. J. Roy. Meteor. Soc.,* **124,** 1071–1107.

Rogers, D. C., P. J. DeMott, and S. M. Kreidenweis, 2001: Airborne measurements of tropospheric ice-nucleating aerosol particles in the Arctic spring. *J. Geophys. Res.,* **106,** 15 053–15 063.

Schramm, J. L., M. M. Holland, J. A. Curry, and E. E. Ebert, 1997: Modeling the thermodynamics of a sea ice distribution, 1: Sensitivity to ice thickness resolution. *J. Geophys. Res.,* **102,** 23 079–23 091.

Shupe, M. D., and J. M. Intrieri, 2004: Cloud radiative forcing of the Arctic surface: The influence of cloud properties, surface albedo, and solar zenith angle. *J. Climate,* **17,** 616–628.

——, T. Uttal, S. Y. Matrasov, and A. S. Frisch, 2001: Cloud water contents and hydrometeor sizes during the FIRE Arctic Clouds Experiment. *J. Geophys. Res.,* **106,** 15 015–15 028.

Slingo, A., 1989: A GCM parameterization for the shortwave optical properties of water clouds. *J. Atmos. Sci.,* **46,** 1419–1427.

Stokes, G. M., and S. E. Schwartz, 1994: The Atmospheric Radiation Measurement (ARM) Program: Programmatic back-

ground and design of the cloud and radiation test bed. *Bull. Amer. Meteor. Soc.,* **75,** 1201–1221.

Tao, X., J. E. Walsh, and W. L. Chapman, 1996: An assessment of global climate model simulations of Arctic air temperatures. *J. Climate,* **9,** 1060–1076.

Turner, D. D., B. M. Lesht, S. A. Clough, J. C. Liljegren, H. E. Revercomb, and D. C. Tobin, 2003: Dry bias and variability in Vaisala RS80-H radiosondes: The ARM experience. *J. Atmos. Oceanic Technol.,* **20,** 117–132.

Twomey, S., 1977: The influence of pollution on the shortwave albedo of clouds. *J. Atmos. Sci.,* **34,** 1149–1152.

Uttal, T., and Coauthors, 2002: The surface heat budget of the Arctic Ocean. *Bull. Amer. Meteor. Soc.,* **83,** 255–275.

Walsh, J. E., V. M. Kattsov, W. L. Chapman, V. Govorkova, and T. Pavlova, 2002: Comparison of Arctic climate simulations by uncoupled and coupled global models. *J. Climate,* **15,** 1429–1446.

Wang, J., H. Cole, D. J. Carlson, E. R. Miller, K. Beierle, A. Paukkunen, and T. K. Lane, 2002: Corrections of humidity measurement errors from the Vaisala RS80 radiosonde—Application to TOGA COARE data. *J. Atmos. Oceanic Technol.,* **19,** 981–1002.

Westwater, E. R., Y. Han, M. D. Shupe, and S. Y. Matrasov, 2001: Analysis of integrated cloud liquid water and precipitable water vapor retrievals from microwave radiometer during SHEBA. *J. Geophys. Res.,* **106,** 32 019–32 030.

Wylie, D., 2001: Arctic weather during FIRE ACE. *J. Geophys. Res.,* **106,** 15 363–15 375.

Yum, S. S., and J. G. Hudson, 2001: Vertical distributions of cloud condensation nuclei spectra over the springtime Arctic Ocean. *J. Geophys. Res.,* **106,** 15 045–15 052.

Zuidema, P., and Coauthors, 2005: An arctic springtime mixed-phase cloud boundary layer observed during SHEBA. *J. Atmos. Sci.,* **62,** 160–176.